



ELSEVIER

Available online at www.sciencedirect.com

SCIENCE @ DIRECT®

Nuclear Instruments and Methods in Physics Research B 230 (2005) 601–607

NIM B
Beam Interactions
with Materials & Atoms

www.elsevier.com/locate/nimb

Detection of acoustic signals induced by heavy-ion impact: ion-beam seismology

Tadashi Kambara *

Atomic Physics Laboratory, RIKEN, Institute of Physical and Chemical Research, 2-1 Hirosawa, Wako, Saitama 351-0198, Japan

Abstract

We study dynamical processes by penetrating radiations inside of bulk solids through the measurements of acoustic waves. We irradiated a solid sample with a single-bunch ion beam of 95 MeV/u Ar ions and observed acoustic signals with piezoelectric sensors. Moving the irradiation position step-by-step on the sample while the sensors were fixed to it, we observed waveforms which propagated at different directions from the source. The angular dependence of acoustic waveforms is analyzed with seismological considerations, and the result shows that the acoustic source in the Ar-irradiation is a nearly isotropic expansion confined in the bulk.

© 2005 Elsevier B.V. All rights reserved.

PACS: 61.80.Jh; 62.30.+d

Keywords: Acoustic emission; Heavy-ion irradiation; Ion beam; Seismic moment

1. Introduction

Radiation penetrating a solid can cause mechanical turbulence and generate elastic waves at ultrasonic frequencies [1]. Several authors have experimentally studied acoustic signals generated by irradiations of electrons, positrons, photons [2,3] and slow ions [4,5]. In contrast to other radiations, a high-energy heavy ion has a large stopping power in matter and the kinetic-energy

deposition has a maximum at the Bragg peak near the end of the range. Therefore main part of the radiation effects can be localized deep in the bulk. Dynamical radiation effects have been studied with various methods like detection of secondary particles (electrons, ions, atoms, clusters) and secondary photons (visible to X-ray), but it is not easy to apply these methods for phenomena deep in solids, since charged particles are stopped and photons are attenuated by thick matter. On the other hand, most solids propagate elastic waves in a long distance, and the waveform is well preserved during propagation since the velocities of

* Tel.: +81 48 462 1111; fax: +81 48 462 4644.
E-mail address: kambara@rarfaxp.riken.jp

the body waves are independent of the frequency. The elastic body wave has two modes with different velocities; the longitudinal, compression wave (P wave) and the transverse, shear wave (S wave) and their amplitudes have different propagation-angle distribution (radiation pattern) depending on the geometry and dynamics at the source.

In spite of a vast difference in energy and geometrical scale between earthquakes and irradiations, seismic waves from earthquakes and acoustic waves from irradiations follow the common theory of elasticity. Although large earthquakes are sometimes disastrous, careful and systematic study of the seismic waves offer almost unique means to investigate the inaccessible interior of the earth, not only the position and dynamical characteristics of the seismic source, but also the internal structure of the earth. We expect that the seismological way can be applicable to the analyses of acoustic signals to know about the elastodynamical aspects of radiation effects. It is non-destructive and real time, in contrast to other methods.

In this report, we show measurements of acoustic waves from solid samples irradiated by 3.8-GeV Ar ions (95 MeV/u). The acoustic waveform and the arrival time were measured at different positions relative to the irradiation point to study the dependence on the propagation direction. Then, applying seismological considerations, we discuss the characteristics of the stress and deformation in solids caused by heavy-ion irradiations. The present results indicate that the deformation caused by the irradiation is nearly isotropic.

2. Experiments

Since the present experimental setup is almost the same as that reported previously [6], we describe it only briefly. A 3.8-GeV Ar beam from RIKEN Ring Cyclotron irradiated a plate of sample. The beam was chopped to a single bunch with width of about 3 ns and rate of about 60 Hz and the timing and the intensity of each bunch of the ions were measured with two secondary-electron monitors on the beam line upstream of the sample. According to the measurement, the number of the

ions per bunch was in the order of 10^3 . The samples were poly-crystalline metal (Al and Cu) and single crystal of BaF₂ which is nearly isotropic in elasticity.

Acoustic signals were detected with two piezoelectric sensors attached to the sample, one on the back and the other on the side. A spring pressed each sensor on the surface of the sample by about 1 kg of force, and vacuum grease was between them for acoustic contact. The sample with the sensors was mounted on a remote-controlled movable feedthrough so that different points on the sample were irradiated.

Fig. 1 schematically shows the geometrical arrangement, where an ion beam from the left impinges on a sample plate with a thickness of D and penetrates it by a range L . In the present condition, the thickness D is about 10 mm. In the previous work [6], we determined the depth of the elastic-wave source by the propagation time and velocity of the acoustic signals, and found that the source position well matched the end of the ion range estimated by a TRIM code [7]. For the range L here we adopt the range of 3.8-GeV Ar ion estimated by the TRIM code, which is 4.24 mm for Al, 1.53 mm for Cu and 3.06 mm for BaF₂. We take the end of the ion range as

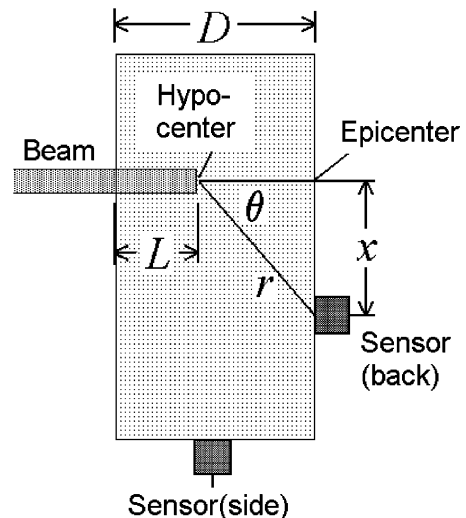


Fig. 1. Geometrical relation between the irradiated sample, the beam and the sensors.

the source of the wave, call it as the hypocenter hereafter, and the point on the back plane just above it as the epicenter. The ultrasonic sensor on the back of the plate is at a distance x from the epicenter E. From the geometry we calculate the distance and the azimuth angle θ between the sensor and the hypocenter.

3. Theoretical seismic motion

We briefly describe the theoretical seismic motion which is the relation between the source motion and the displacement at the surface. Details are found in textbooks of seismology [8]. We treat an infinite, homogeneous and isotropic linear elastic material with a density ρ and Lamé's constants λ and μ . In the following, we use a polar coordinate and a Cartesian coordinate whose axes expressed as x_i ($i = 1, 2, 3$).

The displacement \vec{u} as a function of position and time follows the equation of motion of elastic body:

$$(\lambda + 2\mu)\nabla(\nabla\vec{u}) - \mu\nabla \times \nabla \times \vec{u} + \vec{f} - \rho\ddot{\vec{u}} = 0, \quad (1)$$

where \vec{f} is the force applied per unit volume of the material.

When $\vec{f} = 0$, Eq. (1) yields wave functions for two independent modes of body waves; the P wave is a longitudinal compression wave with a propagation velocity $\alpha = \sqrt{(\lambda + 2\mu)/\rho}$ and the S wave is the shear wave with a velocity $\beta = \sqrt{\mu/\rho}$. Since λ and μ are both positive, the P wave is always faster than the S wave ($\alpha > \sqrt{2}\beta$).

The dynamics in the hypocenter is usually very complicated in natural earthquakes; a sliding motion of a fault following a shear rupture under extreme stress and temperature. To simplify the problem, a kinematical model is often adopted in seismology where the source motion is replaced by an equivalent time-dependent force system applied to the hypocenter. If the hypocenter is contained in the bulk, the net force and torque in the source should be zero, and the force system is a sum of force couples expressed as a 3×3 symmetric tensor called a seismic moment tensor; its diagonal components correspond to the expansion or contraction along the axes, and the non-diagonal

components to shear motions like those in natural earthquakes. In the case of ion-beam irradiation in the direction of axis x_3 , the axial symmetry constrains the elements of the seismic moment to $M_{kl} = 0$ for $k \neq l$ and $M_{11} = M_{22}$. This is expressed as a sum of an isotropic expansion and an expansion/contraction only in the x_3 -direction:

$$M = M_0 f^s(t) \left\{ \begin{pmatrix} 1 & 0 & 0 \\ 0 & 1 & 0 \\ 0 & 0 & 1 \end{pmatrix} + \epsilon \begin{pmatrix} 0 & 0 & 0 \\ 0 & 0 & 0 \\ 0 & 0 & 1 \end{pmatrix} \right\}, \quad (2)$$

where M_0 is the magnitude, $f^s(t)$ denotes the time dependence and ϵ is a parameter which denotes the anisotropy of the expansion.

When the seismic source is at $\vec{\xi}$, the displacement at position \vec{x} and time t is given as

$$u_n(\vec{x}, t) = \int_{-\infty}^{\infty} \sum_{k,l} M_{kl}(\tau) \frac{\partial}{\partial \xi_l} G_{nk}(\vec{x}, t - \tau; \vec{\xi}, 0) d\tau, \quad (3)$$

where G_{nk} is the Green function, and in the present case it is expressed as

$$G_{nk}(\vec{x}, t; \vec{\xi}, 0) = \frac{1}{4\pi\rho r^3} (3r_{,n}r_{,k} - \delta_{nk}) \int_{r/\alpha}^{r/\beta} t' \delta(t - t') dt' + \frac{1}{4\pi\rho\alpha^2 r} r_{,n}r_{,k} \delta\left(t - \frac{r}{\alpha}\right) - \frac{1}{4\pi\rho\beta^2 r} (r_{,n}r_{,k} - \delta_{nk}) \delta\left(t - \frac{r}{\beta}\right), \quad (4)$$

where \vec{r} is the relative position of the observation point \vec{x} from the source $\vec{\xi}$ and $r_{,i} = (x_i - \xi_i)/r$ is the direction cosine.

An isotropic expansion ($\epsilon = 0$) can generate only isotropic P waves and the displacement has only a component in the direction of r as

$$u_r(\vec{x}, t) = \frac{M_0}{4\pi\rho} \left(\frac{1}{\alpha^2 r^2} f^s(t - r/\alpha) + \frac{1}{\alpha^3 r} f^s(t - r/\alpha) \right). \quad (5)$$

The first term is the near-field term whose amplitude decreases as $1/r^2$ and the second one is the far-field term which decreases as $1/r$. An anisotropic expansion only in the x_3 direction,

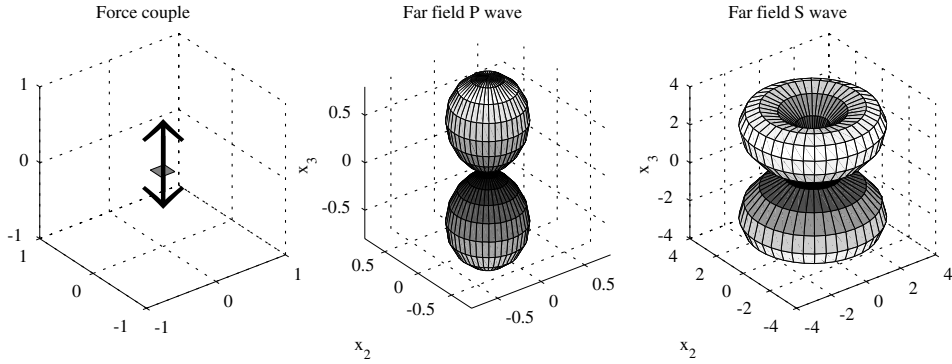


Fig. 2. Amplitude of far-field P wave (middle) and S wave (right) generated by an expansion in the x_3 direction (left). Note that the scale of the amplitude is different between the P and S wave; the P-wave amplitude is five times magnified.

the second term in Eq. (2), results in a displacement:

$$\begin{aligned}
 u_n(\vec{x}, t) = & \frac{M_0}{4\pi\rho} \left[(15r_{,n}\cos^2\theta - 6\delta_{n3}\cos\theta - 3r_{,n}) \right. \\
 & \times \frac{1}{r^4} \int_{r/\alpha}^{r/\beta} t' f^s(t-t') dt' \\
 & + \frac{1}{\alpha^2} (6r_{,n}\cos^2\theta - 2\delta_{n3}\cos\theta - r_{,n}) \frac{1}{r^2} f^s(t-r/\alpha) \\
 & - \frac{1}{\beta^2} (6r_{,n}\cos^2\theta - 3\delta_{n3}\cos\theta - r_{,n}) \frac{1}{r^2} f^s(t-r/\beta) \\
 & + \frac{1}{\alpha^3} r_{,n}\cos^2\theta \frac{\dot{f}^s(t-r/\alpha)}{r} \\
 & \left. - \frac{1}{\beta^3} (r_{,n}\cos^2\theta - \delta_{n3}\cos\theta) \frac{\dot{f}^s(t-r/\beta)}{r} \right], \quad (6)
 \end{aligned}$$

where θ is the angle between \vec{r} and axis x_3 . The last two terms of Eq. (6) correspond to the far-field P and S waves. The both waves have the same time-dependent waveform but the amplitude, propagation speed and angular dependence are different. Since $\alpha > \beta$, the maximum amplitude of the S-wave is larger than that of the P-wave, by a factor of α^3/β^3 .

Fig. 2 shows the amplitude of the P and S waves from the anisotropic expansion in the x_3 direction. The far-field terms in Eq. (6) are calculated as function of the propagation direction for aluminum ($\alpha = 6472$ m/s and $\beta = 3140$ m/s) as an example. The propagation-direction dependence of the amplitude of each wave component is called a radiation pattern.

Both of the radiation patterns in Fig. 2 are symmetric about the beam axis (x_3): The P-wave amplitude has maxima at $\theta = 0^\circ$ and 180° , while the S wave has maxima at 45° and 135° . Since S-wave is not generated by an isotropic expansion, an S wave observed around $\theta = 45^\circ$ should be a clear indication of the anisotropy of the deformation at the seismic source.

When we compare the theoretical radiation patterns with waveforms observed by the sensor in the present experimental setup (Fig. 1), we have to consider two things: Firstly, the distance r increases with θ as $1/\cos\theta$. Secondly, the sensor is sensitive only to the component of the displacement perpendicular to the surface. Therefore, according to the theory, the back sensor observes amplitude of the far-field P-wave from an isotropic expansion (5) as proportional to $\cos^2\theta$. In the case of x_3 -direction expansion, $n = 3$ in (6) gives the observed P-wave amplitude proportional to $\cos^4\theta$ and the S-wave amplitude to $\cos^2\theta\sin^2\theta$.

4. Results

Fig. 3 shows the acoustic waveforms observed with the back sensor on the Al, Cu and BaF₂ samples. Waveforms were recorded at different positions x relative to epicenter and the position was varied by 1 mm-step in a range of $x = \pm 12$ mm. The position is indicated on the right of the graph. The measured waveforms are averaged over 20–50

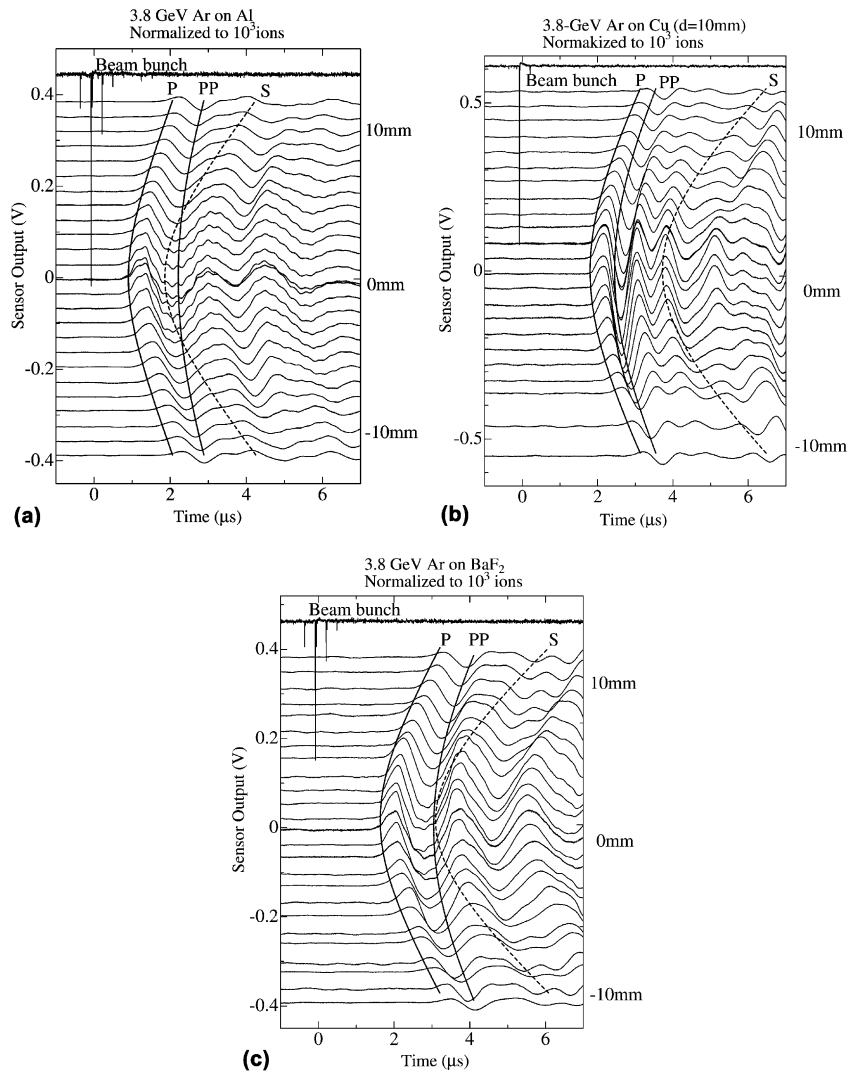


Fig. 3. Acoustic waveforms by 3.8-GeV Ar ions on (a) Al, (b) Cu and (c) BaF₂ observed with the back sensor. P, S and PP denote the calculated arrival times of the direct P wave, direct S wave and P wave after one reflection on the front plane.

shots of ion bunches to reduce noise, and the result is normalized to the same number of ions. In addition to the acoustic waveforms, the typical beam-bunch pattern is shown at the top, and the origin of the time is chosen to the arrival time of the main part of the beam bunch.

The propagation time is shortest at the epicenter ($x = 0$ mm) and it increases with $|x|$. Assuming the hypocenter at the end of the ion range from the TRIM code, we calculate the arrival times of the P and S waves as function of x , using measured val-

ues of sample thickness and the speeds of the waves. The expected P- and S-wave arrival times are drawn in the figure as solid and dashed curves. The onset of the acoustic wave agrees well with the P-wave arrival time for all samples, and the onset is positive pulse, which corresponds to outward motion, with a rise time of about 0.3–0.4 μs . If the deformation at the hypocenter is anisotropic ($\epsilon \neq 0$), an S wave should be observed around $\theta = 45^\circ$ which corresponds to $x = \pm 8.5$ mm for Cu, ± 7 mm for BaF₂ and ± 6 mm for Al. No

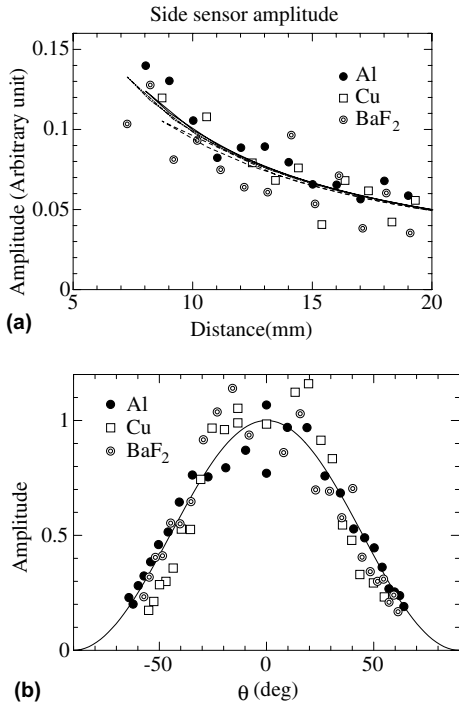


Fig. 4. Onset peak height at the (a) side sensor plotted against the distance from the hypocenter and (b) back sensor plotted against the azimuth angle. Curves are the amplitude estimated for the far-field P-wave from an isotropic expansion.

obvious structure is found along the S-wave arrival-time curve although for BaF₂ the expected S-wave arrival time coincides with a waveform structure which is probably due to reflections in the sensor.

As an index of the P-wave amplitude, we take the height of the onset peak of the waveform and plot it in Fig. 4 for the side and back sensors. Fig. 4(a) shows the amplitude measured by the side sensor where the azimuth angle θ is nearly 90° and only the isotropic component of the seismic tensor contributes to the amplitude. The curve shows the P-wave amplitude expected by the side sensor from a far-field term of an isotropic expansion in Eq. (5). The overall agreement indicates that the far-field term mainly contributes to the observed amplitude and the attenuation of the acoustic signals during the propagation is not significant. Fig. 4(b) shows the amplitude measured by the back sensor as a function of the azimuth angle θ . The

solid line in the figure is a $\cos^2\theta$ curve which is expected from an isotropic expansion. The experimental plots agree the curve fairly well. This angular dependence and the fact that the S-wave is not observed in the waveforms around $\theta = 45^\circ$ indicate that the deformation due to the irradiation is almost isotropic. The upper limit of the anisotropy parameter ϵ has been estimated to be about 0.1 for Al and Cu and 0.4 for BaF₂, where it was more difficult to eliminate the possibility of S-wave overlap because of the structure of the waveform.

5. Conclusions

The acoustic waves have been measured for solid samples of poly-crystalline of Al and Cu and a single crystal of BaF₂ irradiated by short-bunch 3.8 GeV Ar-ions. The irradiation position was scanned on the samples relative to the ultrasonic sensor, so that the dependence on the propagation direction was obtained. For all materials and all directions measured, the P wave is observed in the waveforms, but there is not any clear indication of the S wave. The angular dependence of the observed P wave amplitude is consistent with nearly isotropic emission of the emitted P wave from the hypocenter. These observations indicate that the anisotropy parameter in the seismic moment is smaller than 10% for the Al and Cu samples and 40% for the BaF₂. The deformation induced in the bulk at Bragg peak is more or less isotropic expansion. It is interesting to apply this method in heavier ions with higher stopping power, to study morphology of permanent track and lattice deformation.

Acknowledgments

This experiments have been performed in cooperation with Drs. Y. Kanai, Y. Nakai, T.M. Kojima A. Yoneda and Y. Yamazaki at RIKEN and Prof. K. Kageyama at Department of Mechanical Engineering, Saitama University. One of the coworkers (A.Y.) has also developed the single-bunch beam which has been essential for the present work.

References

- [1] L.M. Lyamshev, *Sov. Phys. Acoust.* 38 (2) (1992) 105.
- [2] B.L. Beron, R. Hofstadter, *Phys. Rev. Lett.* 23 (1969) 184.
- [3] I.A. Borshkovsky, V.D. Volovik, I.A. Grishaev, I.I. Zalyubovsky, V.V. Petrenko, G.A. Chekhutsky, G.L. Fursov, *Phys. Lett. A* 40 (1972) 97.
- [4] D. Adliene, L. Pranevicius, A. Ragauskas, *Nucl. Instr. and Meth.* 209–210 (1983) 357.
- [5] J. Teichert, L. Bischoff, B. Köhler, *Nucl. Instr. and Meth. B* 120 (1996) 311.
- [6] T. Kambara, K. Kageyama, Y. Kanai, T.M. Kojima, Y. Nakai, A. Yoneda, Y. Yamazaki, *Nucl. Instr. and Meth. B* 193 (2002) 371.
- [7] J.F. Ziegler, J.P. Biersack, U. Littmark, *The Stopping and Range of Ions in Solids*, Pergamon Press, New York, 1985.
- [8] T. Lay, T.C. Wallace, *Modern Global Seismology*, Academic Press, New York, 1995 (Japanese translation by T. Yanagidani).